Investigation of spin wave damping in three-dimensional magnonic crystals using the plane wave method

J. Romero Vivas,[1,2] S. Mamica,[1] M. Krawczyk,[1,*] and V. V. Kruglyak[3]

[1]*Faculty of Physics, Adam Mickiewicz University in Poznan, Umultowska 85, Poznan, 61-614 Poland*

[2]*Electrolaer, Godard # 46, Col. Guadalupe Victoria., C.P. 07890, Mexico D.F., Mexico*

[3]*School of Physics, University of Exeter, Stocker Road, Exeter, EX4 4QL, United Kingdom*

(Received 21 August 2012; published 25 October 2012)

The Landau-Lifshitz equation with a scalar damping constant predicts that the damping of spin waves propagating in an infinite homogeneous magnetic medium does not depend on the direction of propagation. This is not the case in materials with a periodic arrangement of magnetic constituents (known as magnonic crystals). In this paper, the plane wave method is extended to include damping in the calculation of the dispersion and relaxation of spin waves in three-dimensional magnonic crystals. A model material system is introduced and calculations are then presented for magnonic crystals realized in the direct and inverted structure and for two different filling fractions. The ability of magnonic crystals to support the propagation of spin waves is characterized in terms of a figure of merit, defined as the ratio of the spin wave frequency to the decay constant. The calculations reveal that in magnonic crystals with a modulated value of the relaxation constant, the figure of merit depends strongly on the frequency and wave vector of the spin waves, with the dependence determined by the spatial distribution of the spin wave amplitude within the unit cell of the magnonic crystal. Bands and directions of exceptionally long spin wave propagation have been identified. The results are also discussed in terms of the use of magnonic crystals as metamaterials with designed magnetic permeability.

DOI: 10.1103/PhysRevB.86.144417 PACS number(s): 75.30.Ds, 75.75.−c, 75.78.−n, 76.90.+d

I. INTRODUCTION

In photonics and phononics, periodic patterning has proven itself as an effective way to obtain materials with custom-made properties. Analogously, materials with a periodic arrangement of magnetic constituents [i.e., magnonic crystals (MCs)], can show properties not found in bulk samples. These crystals can be used for the fabrication of new devices in which spin waves (SWs) act as information carriers. Thus, the investigation of properties of three-dimensional (3D) MCs with nanoscale lattice constants is of both scientific and practical interest. Reviews of possible applications of MCs with modulation at different length scales can be found, for example, in Refs. 1–5.

Loss is an unavoidable property of materials. Hence, it has to be taken into account in the design of magnonic devices and MCs. Studies of the damping of spin waves traveling in thin ferrite films have already been presented.[6,7] Some of the damping effects in one-dimensional MCs have also been discussed in the literature.[8–10] In two-dimensional (2D) MCs, the considerations to include damping effects in the plane wave method (PWM) have been published in Ref. 11. As a continuation of that work, we have implemented loss calculations within the PWM in the case of 3D MCs with the aim of exploring the options for tailoring the intrinsic spin relaxation. It was shown that 3D MCs with lattice constants in nanoscale should have magnonic gaps when constituent ferromagnetic materials are chosen properly.[12,13] This gap can be obtained for many crystal structures, including cubic, simple hexagonal, and close packed lattices.[12,14,15]

The possibility for tailoring damping in magnetic materials is intensively studied in the literature. This direction of research is developed not only in the context of potential applications [e.g., within spintronics (in particular, spin transfer torque devices) and magnonic devices] but also to understand fundamental experimental results in the physics of magnetism.[16–21] There are two contributions to spin relaxation usually identified, intrinsic and extrinsic. The former is usually related to the spin-orbit coupling and is described by the phenomenological Gilbert damping term. In principle, the damping constant can be anisotropic but in 3D metallic ferromagnets under the conditions used in SW calculations this anisotropy is usually averaged out.[22,23] For the extrinsic damping the main contribution is usually attributed to two-magnon scattering processes,[24,25] which can be related to the scattering on defects[26] including also their periodic distribution.[19,27] The influence of the periodic modulation on extrinsic damping processes (i.e., two-magnon scatterings) were studied in Ref. 27. It was shown that a periodic scattering potential for magnons can result in a significant increase in the spin relaxation rates and can enable the tailoring of the anisotropy of damping.[18,27] In another study, the influence of retardation effects on the effective damping was investigated.[28] It was shown that the lifetime of SWs depends on the retardation time and long-living SWs for selected wave vectors were found.

In this paper we show that 3D MCs offer the possibility of tailoring the strength and anisotropy of the intrinsic damping of SWs. We neglect the extrinsic damping as well as any contribution from the surroundings[29] as we assume that the MCs fill the whole space. We also neglect magnetic relaxation due solely to interfaces.[30] The results of our calculations using the above mentioned model are presented for 3D MCs composed of ferromagnetic spheres in a ferromagnetic matrix in a simple cubic (sc) lattice. We assume that in each of the two constituent materials the coefficient of the Gilbert

damping is isotropic, which is a common assumption in the linear approximation used in our calculations.[31]

The layout of this work is as follows. Section II presents the general theory of our calculation method. In Sec. III, we report the calculations using our method for a MC consisting of spherical scattering centers forming a sc lattice. We consider also the effect of material and structural parameter values on the wave damping in this section. The interpretation of the numerical results with the effective and estimated damping coefficients is presented in Sec. IV. Finally in Sec. V we detail how the anisotropy in the effective damping can be used as a tool for designing practical devices.

II. CALCULATION METHOD

The equation of motion of the space- and time-dependent magnetization vector $\mathbf{M}(\mathbf{r},t)$, [i.e., the Landau-Lifshitz-Gilbert equation (LLG)], is the starting point for the study of spin waves in the classical approach. When written in international system of units, it reads

$$\frac{\partial \mathbf{M}(\mathbf{r},t)}{\partial t} = \gamma \mu_0 \mathbf{M}(\mathbf{r},t) \times \mathbf{H}_{\text{eff}}(\mathbf{r},t) + \frac{\alpha}{M_S}\left(\mathbf{M} \times \frac{\partial \mathbf{M}(\mathbf{r},t)}{\partial t}\right). \tag{1}$$

In this equation γ is the gyromagnetic ratio, $\mathbf{H}_{\text{eff}}$ denotes the effective magnetic field acting on the magnetization. We assume that the effective magnetic field is composed of three contributions: bias external magnetic field, exchange field, and magnetostatic field.[32] M_S is the saturation magnetization, μ_0 denotes the permeability of vacuum and the last term on the right describes damping. The dimensionless damping factor α in the rightmost term is Gilbert's phenomenological damping parameter. The LLG equation is nonlinear and to obtain the spin wave spectrum we need to obtain a linear approximation of this equation: we decompose the magnetization vector into a static part (parallel to the external bias magnetic field H_0 with a value equal to the M_S) and a small dynamic part $\mathbf{m}(\mathbf{r},t)$ (the $\mathbf{m}$ vector is perpendicular to H_0). In addition, because we are considering a periodic system, the Bloch theorem is applied. The Fourier transform is used to obtain a frequency domain solution [i.e., we assume $\mathbf{m}(\mathbf{r},t) \propto \exp(i\Omega t)$]. This method, called the plane wave method (PWM), has already been described in the literature, for details see, e.g., Refs. 12 and 13. The methodology for extending the method to consider damping has been described for the 2D case in Ref. 11. Here, we implement the calculation of damping for 3D structures. In the traditional PWM, an eigenvalue problem is obtained and the eigenvalues represent the frequencies, Ω. In the implementation extended to consider damping effects, a generalized eigenvalue problem is obtained and the eigenvalues can adopt complex values (i.e., $\Omega = \Omega' + \mathrm{i}\,\Omega''$) where i is the imaginary unit. The real part of these eigenvalues, Ω' is the frequency, and the imaginary part Ω'' gives the inverse of the SW lifetime (i.e., the decay rate).[33] In the calculations we used 1331 plane waves to obtain reasonable convergence for three low-frequency magnonic bands analyzed in this paper.

The value of the decay rate alone could be used to evaluate the damping at a specific frequency and direction in a wave vector space. On the other hand, considering Eq. (2), which is a known result in the theory of ferromagnetic resonance measurements, we can see that the Gilbert damping parameter in the LLG equation models damping as proportional to the frequency[34]

$$\Delta B_G = 1.16\alpha \frac{\Omega'}{\gamma}, \tag{2}$$

where the B_G is a half width of a ferromagnetic resonance line. It makes sense, therefore, to define a similar quantity that is not proportional to the frequency and therefore allows us to compare the damping modification in the spin wave propagation for different magnonic bands. This quantity will depend on the profile of the magnetization distribution but will not be proportional to the frequency. This quantity, called figure of merit (FOM), was used already in Ref. 11 as the ratio of the real to the imaginary part of the eigenvalues

$$\text{FOM} = \frac{\Omega'}{\Omega''}.$$

The FOM allows us to compare the degree of damping variation between bands and between different directions in space.

In the following section, Sec. III, we define the physical system used to exemplify the use of this 3D PWM including damping and provide representative results.

III. RESULTS OF THE PLANE WAVE METHOD CALCULATIONS

The first system under study is a 3D MC obtained by arranging spherical ferromagnetic scattering centers (material A) in a simple cubic (sc) lattice, as shown in Fig. 1(a). The [001] axis of the crystal is parallel to the z axis. The assumed value of the sc lattice constant is $a = 10$ nm; the magnetic parameters of the matrix material (i.e., material B) in Fig. 1(a) are saturation magnetization $M_S = 0.194 \times 10^6$ A/m and exchange constant $A = 3.996 \times 10^{-12}$ J/m; the magnetic parameters of the spherical scattering centers, material A, are $M_S = 1.752 \times 10^6$ A/m and $A = 2.1 \times 10^{-11}$ J/m. The values assumed for the Gilbert damping parameter were chosen arbitrarily as $\alpha_A = 0.0019$ and $\alpha_B = 0.064$ for spherical scattering centers and the matrix, respectively, unless stated otherwise. This structure will be called *direct crystal*. We will study also the

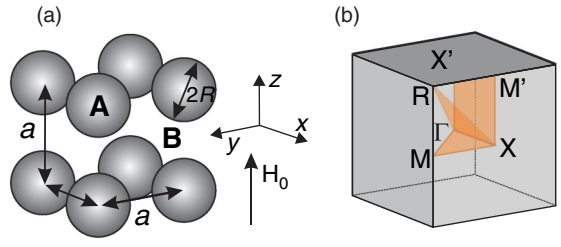

FIG. 1. (Color online) (a) The sc structure of the considered MC (direct crystal). The MC consists of spherical scattering centers (material A of radius R) immersed in the host matrix (material B). The lattice constant is a and the external static magnetic field, H_0 is directed along the z axis. (b) The first BZ of the sc lattice. The dark (orange) color shows the part of the BZ over which the calculations of the magnonic structure are performed.

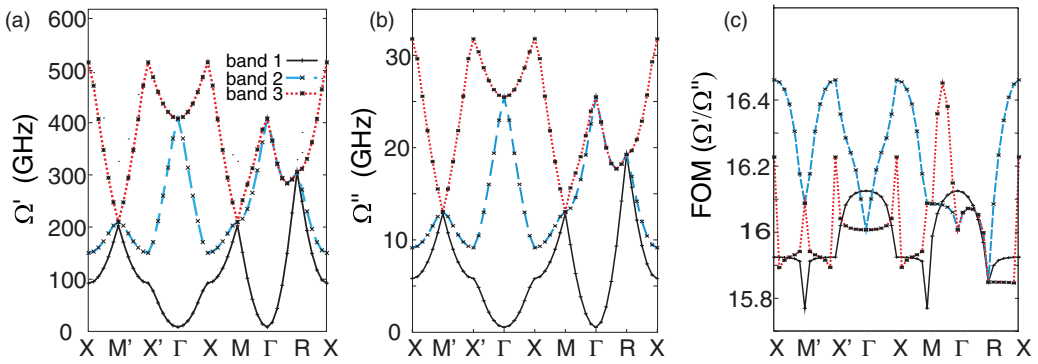

FIG. 2. (Color online) The frequency and decay rate of the SWs are shown for the direct MC (spheres of material A in matrix B) in (a) and (b), respectively. A filling fraction of 0.2 was assumed in the calculations. (c) The figure of merit (FOM) is shown for the same structure.

corresponding *inverted crystal* (i.e., a crystal with scattering centers made of materials B and A serving as the matrix material). A constant external magnetic field $\mu_0 H_0 = 0.3$ T is applied in the z direction to saturate the crystal. The dynamic part of the precessing magnetization has only x and y nonzero components.

The magnonic band structure resulting from the numerical solution of the eigenproblem for the direct MC is shown in Fig. 2. The filling fraction, defined as a ratio of the volume of scattering centers in the unit cell (it is a sphere in our case) to the volume of the unit cell: $f = 4\pi R^3/3a^3$, was assumed to be $f = 0.2$. It corresponds to a sphere radius $R = 3.628$ nm. The magnonic band structure was calculated along a path in the irreducible part of the first Brillouin zone (BZ). The points along this path are defined in Fig. 1(b). We limit the spectra presented in this paper to low frequencies only (i.e., to the first three bands). We show the frequency (Ω') and decay rate (Ω'') in dependence on the wave vector in Figs. 2(a) and 2(b), respectively. We can see that there is not any magnonic band gap in the frequency spectra. We also observe similar wave vector dependencies for the frequencies and decay rates. This implies that the FOM should be quite uniform in the whole BZ. This is confirmed by Fig. 2(c) in which the FOM is shown along the path in the first BZ. The FOM has values in the range from 15.8 to 16.4. In this case the FOM can therefore be regarded as nearly isotropic for all of the considered low-frequency bands.

Let us now increase the filling fraction in the direct structure. In Figs. 3(a) and 3(b) we show the corresponding magnonic band structure (i.e., the frequency and decay rate) respectively, for the direct MC with $f = 0.5$ ($R = 4.92$ nm). We found the magnonic band spectrum to be quite different to that for $f = 0.2$. In particular, the first band is separated from the upper bands in most of the first BZ except for the R-X direction, thereby forming a partial band gap. The wave vector dependence of the decay rate for the first band follows that of the frequency. Consequently, we obtain an almost constant FOM [note the scale of the vertical axis in Fig. 3(c)]. For the second band, we found that around the Γ point, where Ω' has a maximum, Ω'' has the minimum. As a result of this, the FOM is very large near the center of the BZ, reaching nearly 160. In the rest of the BZ, the FOM is below 30. The FOM is strongly dependent on the value of the wave vector but remains almost independent on the direction of propagation.

Thus, we have found that a partial band gap in the magnonic spectrum and significant values of the FOM coexist at some points in the BZ. We have performed calculations for other filling fractions from 0 up to the value corresponding to the close-packed structure ($f = 0.523$) for the direct crystal and no full gap was found. Nevertheless, a full band gap is observed for the inverted crystal structure. In Figs. 4(a) and 4(b) we show Ω' and Ω'' as a function of the wave vector along a path in the first BZ for the inverted MC with filling fraction of 0.5.

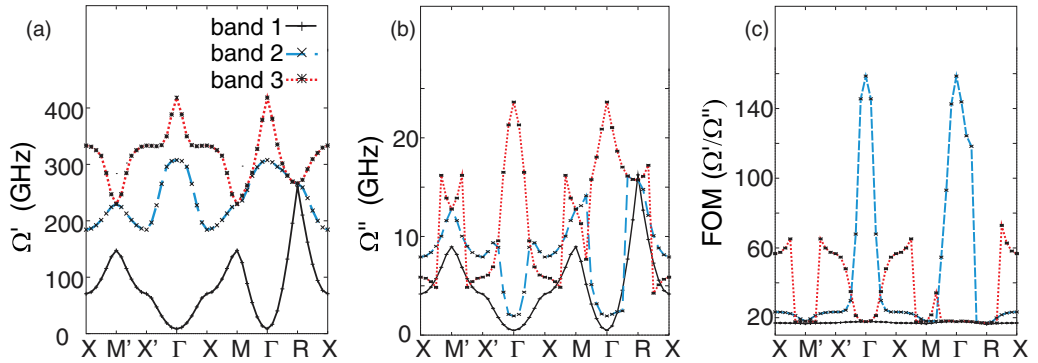

FIG. 3. (Color online) The frequency and decay rate of SWs in the first BZ for a direct MC (spheres of material A in a matrix of material B) are shown in (a) and (b), respectively. A filling fraction 0.5 was assumed in calculations. (c) Figure of merit (FOM) for the same structure.

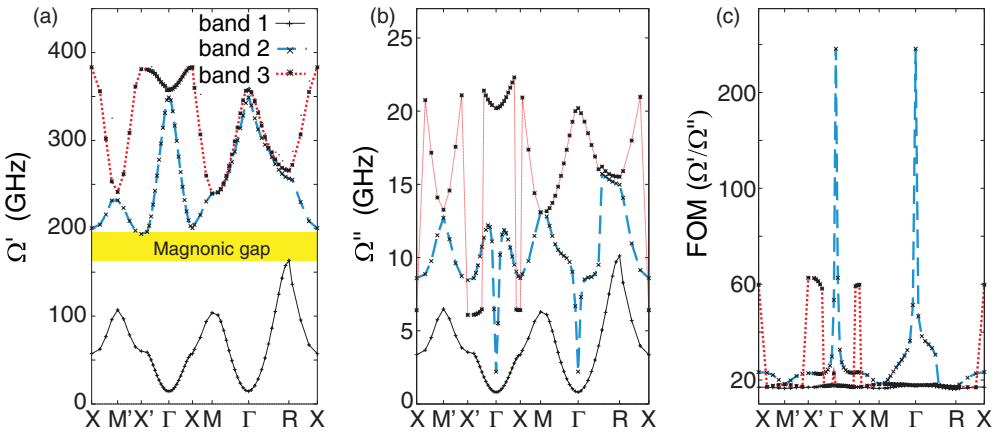

FIG. 4. (Color online) The frequency and decay rate of SWs in the first BZ for an inverted MC (spheres of material B in a matrix of material A) are shown in (a) and (b), respectively. A filling fraction of 0.5 was assumed in the calculations. (c) The FOM is shown for the same structure.

We found a complete magnonic band gap between the first and second bands. We also found that, in this case, the FOM has very small values for the first band. These values are nearly independent on the propagation direction or the magnitude of the wave vector. On the other hand, the second band reaches a significantly higher value of the FOM at the Γ point (up to 250). This value is much larger than that observed for the direct structure [Fig. 3(c)]. However, the FOM is again almost isotropic and has a sharp peak exactly at the center of the BZ (i.e., because the dispersion curve is flat and the group velocity of SWs goes through zero).

From the results presented so far, we can see that significant values of the FOM are associated with the second band (i.e., two absolute magnonic band gaps are found). In the previously presented spectra, the lowest band is separated from the second one by a magnonic gap. Figure 5 shows the magnonic spectra for the inverted crystal with a filling fraction of 0.2, with Ω' and Ω'' plotted as a function of the wave vector in panels (a) and (b), respectively. Both band gaps are marked in yellow color in the figure. These two band gaps separate the second band from the other magnonic bands. The imaginary part of the frequency shows features that are not present in the other crystals investigated here. For the second band, Ω' has a maximum at the Γ point, and consequently, the FOM has a minimum in the same point. The maximal values of the FOM, larger than 400, are found at corners and edges of the first BZ [i.e., at the points $M = \pi/a(1,1,0)$, $M' = \pi/a(1,0,1)$, and $R = \pi/a(1,1,1)$]. At the borders of the first BZ along the principal axis [$X = (1,0,0)$ and $X' = (0,0,1)$] we found the FOM to reach only values that are smaller than 200. We can conclude that in this crystal, the FOM is anisotropic and strongly dependent on the magnitude of the wave vector.

In summary, we have found:

(i) A low value of the FOM is observed for the first band both for direct and inverted crystals irrespectively of the filling fraction. The FOM is almost isotropic and only weakly dependent on the absolute value of the wave vector. This means that this band can be described using effective parameters.

(ii) Only for the inverted crystal with $f = 0.2$ we found strong anisotropy in the FOM for the second band.

(iii) There is apparently a cause-and-effect relationship between the isolation of the second band (due to the presence of band gaps directly above and below) and the observation of high values of the FOM.

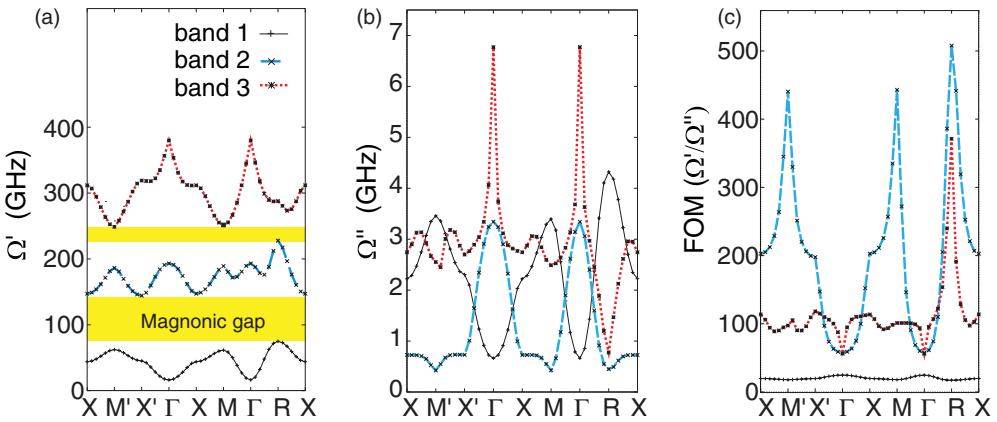

FIG. 5. (Color online) The real and imaginary parts of the frequency in the first BZ for inverted MC (spheres of material B in matrix of material A) in (a) and (b), respectively. A filling fraction of 0.2 was assumed in the calculations. (c) The FOM is shown for the same structure.

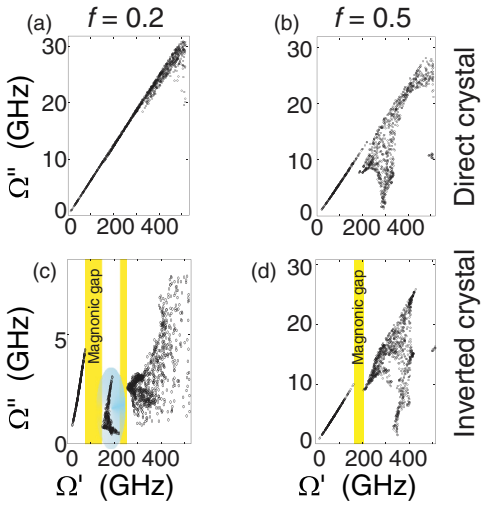

FIG. 6. (Color online) Decay rate of SWs versus its frequency for wave vectors randomly chosen from the first BZ. Direct crystals (A spheres in the B matrix) are shown in (a) and (b), inverted crystals (B spheres in the A matrix) in (c) and (d). In (a) and (c) the results for $f = 0.2$ and in (b) and (d) for $f = 0.5$ are shown. Magnonic gaps are colored in yellow color. In (c) the second band with the moonlike shape is marked by blue ellipse, as it is expected to have strong anisotropy in damping.

IV. DISCUSSION

It has already been mentioned that MCs showing a strong dependence of loss on the direction of the wave vector can be used to design effective magnonic waveguides.[11] We would like to focus on the anisotropy of lifetime of SWs from another point of view and to explain the physical mechanisms that govern the damping of SWs in MCs. To facilitate the analysis, we propose to plot the decay rate versus frequency of the SWs as calculated for wave vectors of random direction and magnitude in the first BZ. Figure 6 shows such plots for the direct and inverted MCs with filling fractions $f = 0.2$ and 0.5. From these figures we find two linear dependencies: a linear function Ω'' vs. Ω' for the first mode and a linear dependence of the upper limit of $\Omega'' \equiv \Omega''_{\max}$ on Ω' for all the considered structures.[35]

The linear relation between the decay rate of SWs and the frequency for the first band can be described by the following relation: $\Omega'' = \mathrm{FOM}^{-1} \times \Omega'$. We found the inverse of FOM to be the slope of the straight line obtained by regression of the data presented in Fig. 6. To explain this feature let us consider SWs propagating in uniform materials. To have a good model for comparison we have to choose a proper structure. Because we are studying 3D MCs filling the whole space, the proper choice seems to be the ferromagnetic uniformly magnetized sphere with free boundary conditions imposed on the dynamic component of the magnetization vector. The sphere is considered in order to avoid shape anisotropy effects. If the sphere is small enough to separate higher harmonics from the uniform excitation, such results should be useful for interpretation of the dependencies found for low-frequency modes in 3D MCs, at least. In uniformly magnetized spheres, $\mathrm{FOM} = 1/\alpha$, where α is a Gilbert damping constant of the uniform sphere.[33] This means that the lifetime of SWs from the first band of 3D MCs behaves like the one from uniform materials. This allows us to introduce the effective damping of the low-frequency mode in 3D MCs as $\alpha_{\mathrm{eff}} = 1/\mathrm{FOM}$, where the inverse of FOM is the slope of the line fitted to the dependencies shown in Fig. 6 for the first band. From the PWM solutions we have found α_{eff} equal: 0.062, 0.058, 0.052, and 0.059 for the direct crystal $f = 0.2$ and 0.5, and inverted crystals with $f = 0.2$ and 0.5, respectively. These values are between the values of the Gilbert damping coefficient of the constituent materials (α_{A} and α_{B}) but in fact all of them are very close to the highest value (i.e., 0.064). This behavior would be reasonable if the SW modes from the first band in both kinds of the investigated crystals concentrated their amplitude mainly in the material with higher value of damping. Two-dimensional color maps of the modulus of the dynamical components of the magnetization vector (i.e., $|\mathbf{m}| = \sqrt{m_x^2 + m_y^2}$) are shown in Fig. 7 , confirming our hypothesis. The amplitude is shown in two cross sections perpendicular to the z axis: one plane crossing the centers of the spheres [plane (001)] and the second crossing the space in the middle between the spheres [plane (002)]. Red color marks maximum values while blue corresponds to zeros of the amplitude.

To have a quantitative measure of the damping of SW modes we can integrate the mode profiles in Fig. 7 weighted with the respective damping. The derivation of the formula for an estimated damping α_{est} in one-dimensional periodic structures can be found in Ref. 36. A similar procedure can be applied to 3D structures and the final expression will have a similar form with integrals over volume of the material A or B in the unit cell, now in 3D,

$$\alpha_{\mathrm{est}}(\mathbf{k},n) = \frac{\frac{\alpha_{\mathrm{sph}}}{M_{\mathrm{S,sph}}}\int_{\mathrm{sph}} |\mathbf{m}_{\mathbf{k},n}|^2 dv + \frac{\alpha_{\mathrm{mat}}}{M_{\mathrm{S,mat}}}\int_{\mathrm{mat}} |\mathbf{m}_{\mathbf{k},n}|^2 dv}{\frac{1}{M_{\mathrm{S,sph}}}\int_{\mathrm{sph}} |\mathbf{m}_{\mathbf{k},n}|^2 dv + \frac{1}{M_{\mathrm{S,mat}}}\int_{\mathrm{mat}} |\mathbf{m}_{\mathbf{k},n}|^2 dv}, \quad (3)$$

where the indices "sph" and "mat" make reference to the sphere and matrix, respectively; $\mathbf{m}_{\mathbf{k},n}$ is the dynamical component of the magnetization vector for the band n and wave vector $\mathbf{k}$. This formula allows us to calculate an estimated value of damping for each band (n) and each wave vector ($\mathbf{k}$). The calculated values of the estimated damping parameters for the first band in Γ and R points in the BZ are collected together with the effective damping constants obtained from the slopes in Fig. 6 in Table I. For the direct crystal the damping constant from both methods match very well. For the inverted crystal, there is significant variation of α in dependence on the wave vector value [see also Fig. 5(c)] but the arithmetic average of estimated values also match well with the α_{eff}.

Now we will discuss the results obtained for the second band, where in the case of the inverted crystals, a large FOM was found in the R and M points in the BZ. The amplitude of the dynamical components of the magnetization vector and the respective estimated damping parameters are shown in Fig. 7 for the wave vector from the BZ center and BZ edge (i.e., for the Γ and R points) respectively, for the direct crystal ($f = 0.5$) and inverted crystal ($f = 0.2$). The estimated damping parameters α_{est} from the profiles are given also in this figure. For the direct crystal we have found that the FOM reaches a high value at the Γ point ($\cong$160) and a very small value for the R point (less than $\cong$18), as shown in Fig. 3(c). The respective damping values obtained from the profiles are 0.006 and 0.063,

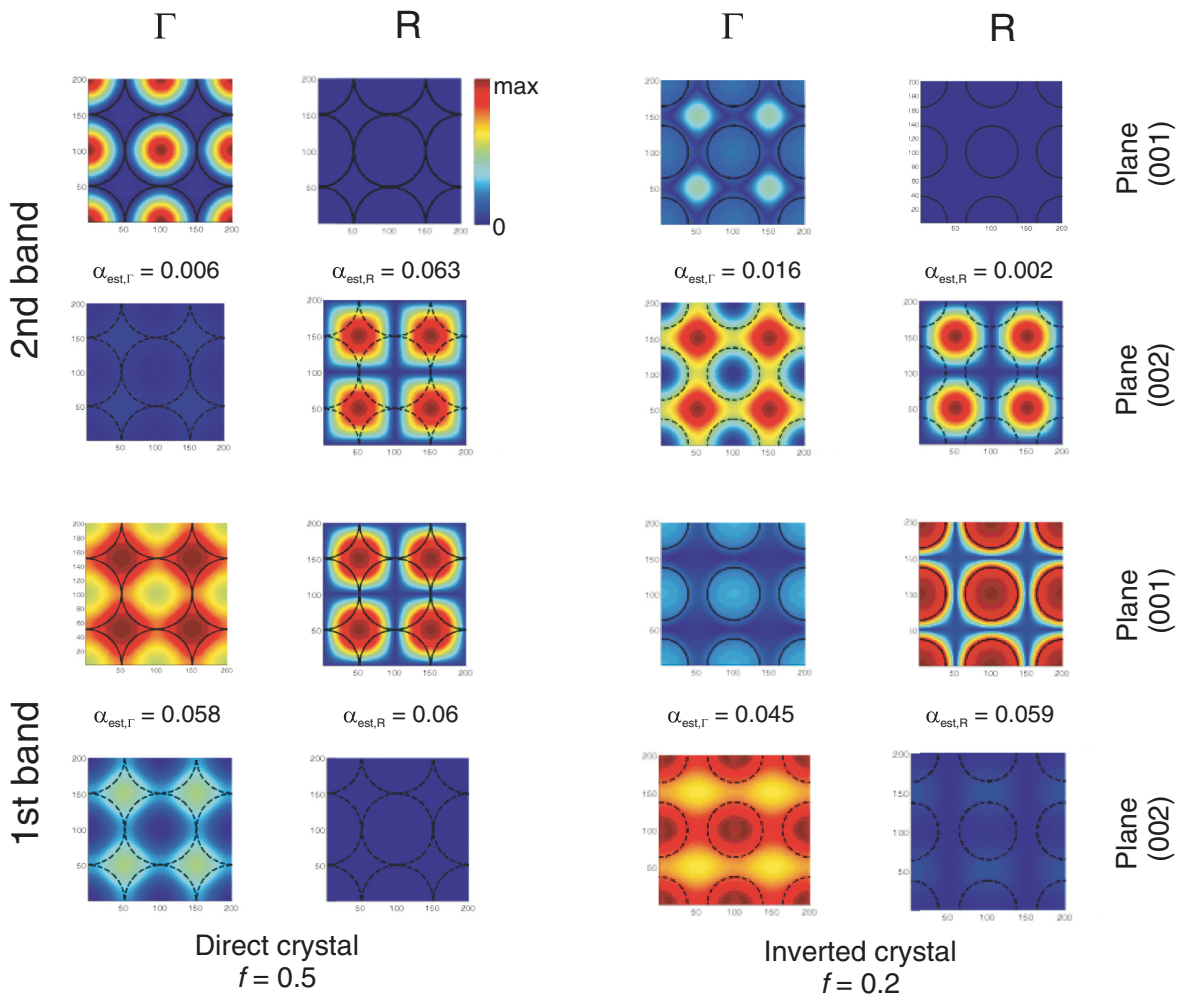

FIG. 7. (Color online) The amplitude of the dynamical components of the magnetization vector across the planes perpendicular to the z axis and crossing it at 0 [plane (001)] and at $a/2$ [plane (002)]. The profiles from the first and the second band in Γ and R point are shown for the direct crystal with $f = 0.5$ (left columns) and for the inverted crystal and $f = 0.2$ (right columns). The estimated value of the damping constant of the related mode [calculated according to Eq. (3)] is also given for each profile.

for the Γ and R points, respectively. For the inverted structure a strong change in the FOM, which is eight times lower at the Γ point as compared to its value at the R point can be seen in Fig. 5(c). This fact is also supported by the damping coefficient values obtained from the SW profiles: $\alpha_{\rm est}(\Gamma,2) = 0.016$ and $\alpha_{\rm est}(R,2) = 0.002$ at Γ and R point in the BZ, respectively.

TABLE I. The effective damping parameters ($\alpha_{\rm eff}$) for the first band obtained by assuming a linear dependence $\Omega''(\Omega')$ and fitting the slope from Fig. 6 are shown. The estimated damping coefficients ($\alpha_{\rm est}$) extracted according to Eq. (3) from the profiles of SWs at the Γ and R points in the first BZ for the first band shown in Fig. 7 are also presented.

Structure		$\alpha_{\rm eff}$	$\alpha_{\rm est}(\Gamma,1)$	$\alpha_{\rm est}(R,1)$
Direct	$f = 0.5$	0.058	0.058	0.06
Inverted	$f = 0.2$	0.052	0.045	0.059

We have already established the relation between the value of the FOM, estimated values of the damping coefficients, and the distribution of the mode profiles over the constituent materials. It remains still unattended, however, how changes in the damping parameters of the constituent materials ($\alpha_{\rm A}$ and $\alpha_{\rm B}$) influence the lifetime of the different modes. To get some insight we propose to take a look at the frequency and decay rate as a function of the relative loss parameter (RLP), which takes values from 0 to 1 and we define as

$$\begin{aligned} \alpha_{\rm sph} &= 0.0659 \times {\rm RLP}, \\ \alpha_{\rm mat} &= 0.0659 \times (1.0 - {\rm RLP}), \end{aligned} \tag{4}$$

where the coefficient 0.0659 is chosen equal to $\alpha_{\rm A} + \alpha_{\rm B}$. According to this definition, for RLP = 0 the SWs in spheres will be undamped while the damping will reach its maximal value (i.e., 0.0659) in the matrix. For RLP = 1, the reverse situation occurs (i.e., no damping is present in the matrix) while it reaches its maximum value in the spheres. In Figs. 8(a) and 8(b) the frequency and decay rate of SW modes from the

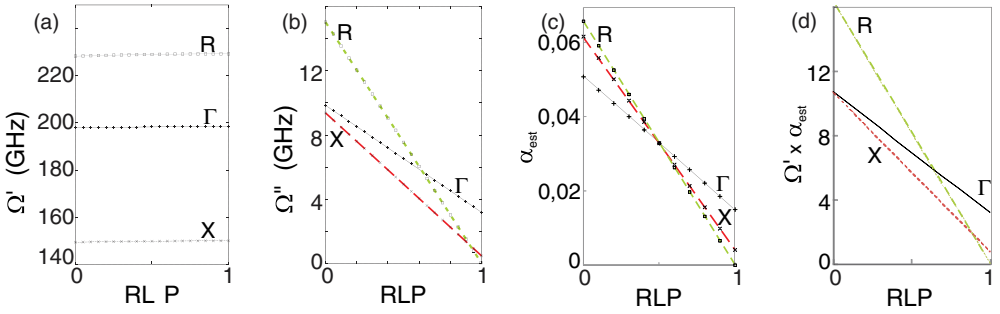

FIG. 8. (Color online) (a) Frequency and (b) decay rate of the SWs are shown as a function of the RLP for the inverted crystal with filling fraction 0.2 calculated with PWM. The frequencies from the second band for the Γ, *R*, and *X* points in the BZ are shown. (c) Estimated values of the damping coefficient are shown in dependence on RLP for the Γ, *X*, and *R* points for the second band. α_{est} are calculated according to Eq. (3). (d) The product of α_{est} and Ω' is shown for the Γ, *X*, and *R* points from the second band. There is a close relation between $\alpha_{est} \times \Omega'$ [shown in (d)] and Ω'' [shown in (b)].

second band for three points from the first BZ (i.e., for Γ, *X*, and *R*) are shown in dependence on the RLP. The calculations were performed for the inverted crystal with filling fraction 0.2. We have found that the frequency is virtually independent on the RLP [Fig. 8(a)]. This behavior can be expected due to the fact that in thin films the dependence of damping on frequency is a second-order effect.[33] The decay rate is a linear function of the RLP with negative slope depending on the wave vector: at the *R* point the slope reaches its highest value while at the Γ point, it reaches its lowest value. We can understand this behavior, because we already showed that the amplitude of the SW modes for the second band is concentrated mainly in the spheres. Consequently, it is expected to observe the lowest values of Ω'' for RLP $= 1$.

The RLP of the inverted crystal [the corresponding band structure is shown in Fig. 5(a)] is 0.97. We see that for this RLP, the imaginary part of a frequency at *R* and *X* has almost the same value but less than half of that at Γ point. This shows from another point of view the main features already observed in Fig. 5(c) (i.e., highest FOM at *R* and smallest at Γ). Here we see that the anisotropy of the FOM is dependent on the distribution of damping among the constituent materials of the MC. In particular, no anisotropy is observed for the case when RLP $= 0.5$ (i.e., when the damping coefficients in spheres and matrix are equal). This result can also be obtained directly from the PWM [i.e., by plotting $FOM(\text{RLP}) \equiv \Omega'(\text{RLP})\Omega''(\text{RLP})$].

The linear dependencies presented in Fig. 8(b) provide evidence that the estimated damping coefficient calculated from the Eq. (3) should also preserve a linear dependence on the RLP. The α_{est}(RLP) can be calculated from the SW profiles obtained from PWM (the profiles have to be calculated only once for selected RLP) according to Eq. (3) with damping coefficients defined by Eqs. (4). The results for the second band for a few selected points in the BZ are shown in Fig. 8(c). We see that for RLP $= 0.5$ the α_{est} is the same independently of the wave vector. To have a quantitative comparison between α_{est} and the numerically calculated Ω'' we need to multiply α_{est} by Ω'. The product $\alpha_{est} \times \Omega'$ is shown in Fig. 8(c). A good qualitative agreement with Ω'' as shown in part (b) of this figure is clear. Quantitatively, the differences are largest near RLP $= 0$ and decrease when the RLP increases.

V. APPLICATION OF THE PROPOSED THREE-DIMENSIONAL MAGNONIC CRYSTAL

In Fig. 6(c) a shape similar to a crescent moon can be observed for the second band lying between two magnonic band gaps. This is interesting because it means that, depending on the direction, we can identify regions of low and high damping for the same frequency and nothing in between. For application as beam shaper, this is just what we need. The region in which this happens is easy to identify using the introduced style of plotting. Also, it allows us to identify propagation directions that correspond to low and high damping at the same frequency. We can use Fig. 5 for this purpose, where the respective band structure is shown. We can note that on the paths going through Γ point (i.e., from X' to Γ to *X* and from *M* to Γ to *R*, the decay rate is higher (and consequently the FOM is smaller) than in the rest of the path. We can also notice that for frequencies above approximately 200 GHz there is an allowed SW band only around the *R* point. In this point also the decay rate is very low, giving high FOM. This functionality can be combined with changes controlled by the external magnetic field, which would have the effect of shifting up or down the range of frequencies where the above mentioned conditions are fulfilled.

If we want to use a mode for transmitting information, in other words, if we want to use our infinite MC as a waveguide, a necessary condition for usefulness is to show that the group velocity (i.e., its magnitude) is greater than zero. The extremal values of the FOM are found for values of the wave vectors in the BZ border (*R*, *X*, or *M* points) or at the BZ center (Γ point). At these points the dispersion curves reach extreme values and the group velocity is 0. To have a qualitative measure of the usefulness of a given mode we propose to look at the product of the group velocity and the FOM. A large value of this product will occur at points with low loss and high group velocity. In Fig. 9 we show the product, $v_g \times$ FOM (calculated directly from the dispersion relation) for the second band along the path in

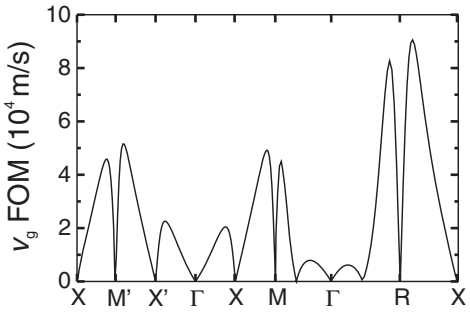

FIG. 9. The absolute value of the product of a group velocity (v_g) and FOM for the second band for the inverted crystal (with $f = 0.2$) along the path in the first BZ.

the first BZ for the inverted crystal with $f = 0.2$. We see, that on the path along, Γ-R and X-R this product has maxima, which define the optimal wave vectors for possible applications. At these points the group velocity of SWs is around 200 m/s. This speed is rather low, but still a lifetime around 0.5 GHz will allow a transport of the signal for a distance around 2 μm. This application would also face the challenge that the anisotropy of the damping in 3D MCs will depend on the RLP as shown in Figs. 8(b) and 8(c). This means that the properties depend on the distribution of damping among the constituent materials. This however could also be considered as an opportunity from the designer point of view.

In Ref. 37, Mruczkiewicz *et al.* showed that stacks of 2D all-ferromagnetic magnonic crystals could be used to design metamaterials with negative permeability at frequencies of several tenths of GHz. In particular, negative permeability was observed in the vicinity of high-order resonances for which the magnonic mode amplitude was preferentially distributed within one of the two constituent materials. The results presented in this paper allow us to speculate that if this material in which the magnonic amplitude is concentrated is in addition characterized by a low damping coefficient, then the resonance will be even stronger and the quality factor will be even higher than that obtained in Ref. 37. A rigorous proof of this hypothesis is however beyond the present study.

VI. CONCLUSION

Using numerical calculations based on the PWM we have shown that magnonic crystals enable us to tailor the effective intrinsic damping of spin waves. A proper choice of the MC structure and its filling fraction allows us to design a magnonic band structure with anisotropic and strongly wave-vector-dependent effective damping. We introduced the plots of the decay rate versus frequency for randomly chosen wave vectors from the first BZ. With the help of these plots we have shown that it is possible to obtain for the same frequency two different directions of SW propagation with low and high damping, where propagation takes place at a finite group velocity.

We have proposed a qualitative explanation of the dependencies observed in our numerical results based on the analysis of the SW amplitude distribution among the constituent materials. The formula for the estimated effective damping coefficient, introduced here for 3D MCs, is wave vector and band number dependent and describes adequately numerical results. We have shown that the decay rate of SW in 3D MCs is a linear function of the relative loss parameter. This is an important result, which allows for a reduction of the time of computations. We have shown also that large values of the FOM in MCs coexist with magnonic gaps in the spin wave spectra as both effects are influenced by the distribution of the SW amplitude in the unit cell in a similar way. This model allows us to understand the effective behavior of damping of the first mode in the magnonic spectrum, irrespective of the direction and magnitude of the wave vector.

ACKNOWLEDGMENTS

The research leading to these results has received funding from the European Community's Seventh Framework Programme (Grant No. FP7/2007-2013) under Grant Agreements No. 247556 (People), NoWaPhen and No. 233552, DYNAMAG project. V.V.K. also acknowledges funding received from EPSRC of the UK under Project No. EP/E055087/1. The calculations presented in this paper were performed in Poznan Supercomputing and Networking Center.

*krawczyk@amu.edu.pl

[1] A. A. Serga, A. V. Chumak, and B. Hillebrands, J. Phys. D: Appl. Phys. **43**, 264002 (2010).
[2] S. Neusser and D. Grundler, Adv. Mater. **21**, 2927 (2009).
[3] V. V. Kruglyak, S. O. Demokritov, and D. Grundler, J. Phys. D **43**, 260301 (2010).
[4] A. Khitun, M. Bao, and K. L. Wang, J. Phys. D **43**, 264005 (2010).
[5] S.-K. Kim, J. Phys. D **43**, 264004 (2010).
[6] D. D. Stancil, J. Appl. Phys. **59**, 218 (1986).
[7] D. D. Stancil and A. Prabhakar, *Spin Waves* (Springer, Berlin, 2009).
[8] V. V. Kruglyak and A. N. Kuchko, Phys. Met. Metallogr. **92**, 211 (2001).
[9] V. V. Kruglyak and A. N. Kuchko, J. Magn. Magn. Mater. **272-276**, 302 (2004).
[10] V. V. Kruglyak and A. N. Kuchko, Phys. Met. Metallogr. **93**, 511 (2002).
[11] R. P. Tiwari and D. Stroud, Phys. Rev. B **81**, 220403 (2010).
[12] M. Krawczyk and H. Puszkarski, Phys. Rev. B **77**, 054437 (2008).
[13] S. Mamica, M. Krawczyk, M. L. Sokolovskyy, and J. Romero Vivas, Phys. Rev. B **86**, 144402 (2012).
[14] M. Krawczyk and H. Puszkarski, Cryst. Res. Technol. **41**, 547 (2006).
[15] M. Krawczyk, J. W. Klos, M. L. Sokolovskyy, and S. Mamica, J. Appl. Phys. **108**, 093909 (2010).
[16] C. Le Graët, D. Spenato, S. P. Pogossian, D. T. Dekadjevi, and J. Ben Youssef, Phys. Rev. B **82**, 100415 (2010).

[17]I. Barsukov, R. Meckenstock, J. Lindner, M. Möller, C. Hassel, O. Posth, M. Farle, and H. Wende, IEEE Trans. Magn. **46**, 2252 (2010).
[18]I. Barsukov, P. Landeros, R. Meckenstock, J. Lindner, D. Spoddig, Z.-A. Li, B. Krumme, H. Wende, D. L. Mills, and M. Farle, Phys. Rev. B **85**, 014420 (2012).
[19]P. Landeros and D. L. Mills, Phys. Rev. B **85**, 054424 (2012).
[20]K. Sekiguchi, T. N. Vader, K. Yamada, S. Fukami, N. Ishiwata, S. M. Seo, S. W. Lee, K. J. Lee, and T. Ono, Appl. Phys. Lett. **100**, 132411 (2012).
[21]L. Lu, J. Young, M. Wu, C. Mathieu, M. Hadley, P. Krivosik, and N. Mo, Appl. Phys. Lett. **100**, 022403 (2012).
[22]J. Kuneš and V. Kamberský, Phys. Rev. B **65**, 212411 (2002).
[23]J. Seib, D. Steiauf, and M. Fähnle, Phys. Rev. B **79**, 092418 (2009).
[24]R. Arias and D. L. Mills, Phys. Rev. B **60**, 7395 (1999).
[25]J. Dubowik, K. Zaleski, H. Glowinski, and I. Goscianska, Phys. Rev. B **84**, 184438 (2011).
[26]G. Woltersdorf and B. Heinrich, Phys. Rev. B **69**, 184417 (2004).
[27]I. Barsukov, F. M. Römer, R. Meckenstock, K. Lenz, J. Lindner, S. Hemken to Krax, A. Banholzer, M. Körner, J. Grebing, J. Fassbender, and M. Farle, Phys. Rev. B **84**, 140410 (2011).
[28]T. Bose and S. Trimper, Phys. Rev. B **83**, 134434 (2011).
[29]Y. Tserkovnyak, A. Brataas, and G. E. W. Bauer, Phys. Rev. Lett. **88**, 117601 (2002).
[30]B. Heinrich, R. Urban, and G. Woltersdorf, J. Appl. Phys. **91**, 7523 (2002).
[31]K. Gilmore, M. D. Stiles, J. Seib, D. Steiauf, and M. Fähnle, Phys. Rev. B **81**, 174414 (2010).
[32]We use here the same formulations for the exchange and magnetostatic fields as in Ref. 12.
[33]A. G. Gurevich and G. A. Melkov, *Magnetization Oscillations and Waves* (CRC Press, Boca Raton, 1996).
[34]K. Zakeri, J. Lindner, I. Barsukov, R. Meckenstock, M. Farle, U. von Hörsten, H. Wende, W. Keune, J. Rocker, S. S. Kalarickal, K. Lenz, W. Kuch, K. Baberschke, and Z. Frait, Phys. Rev. B **76**, 104416 (2007).
[35]For the inverted crystal with $f = 0.2$ shown in the Fig. 6(c) due to limiting range of presented points the linear dependence of the upper limit is not clear. But for higher frequencies (decaying rates) this linear dependence is still present.
[36]A. M. Zyuzin, A. G. Bazhanov, S. N. Sabaev, and S. S. Kidyaev, Phys. Solid State **42**, 1279 (2000).
[37]M. Mruczkiewicz, M. Krawczyk, R. V. Mikhaylovskiy, and V. V. Kruglyak, Phys. Rev. B **86**, 024425 (2012).